ORIGINAL RESEARCH

Extraction, characterization and chemical functionalization of phosphorylated cellulose derivatives from Giant Reed Plant

Anass Ait Benhamou · Zineb Kassab · Mehdi Nadifiyine · Mohamed Hamid Salim · Houssine Sehaqui · Amine Moubarik · Mounir El Achaby

Abstract In this work, cellulose microfibers (CMFs) and cellulose nanocrystals (P-CNCs) having phosphoric groups on their surfaces were prepared by phosphorylation of cellulose extracted from Giant Reed plant, using ammonium dihydrogen phosphate (NH_4-H_2PO_4) in a water-based urea system and phosphoric acid (H_3PO_4) without urea as phosphorous agents, respectively. Phosphorylated samples were studied in terms of their charge content, chemical structure, crystallinity, morphology, and thermal stability using several characterization techniques. Conductometric titration results showed higher charge content after phosphorylation with urea for P-CMFs about 3133 mmol kg^{-1}, while without urea P-CNCs exhibited 254 mmol kg^{-1}. FTIR analysis confirmed the total removal of non-cellulosic compounds from microfibers' surface and their partial oxidation after phosphorylation. XRD analysis proved that the P-CMFs and P-CNCs exhibited cellulose I structure, with a crystallinity index of 70 and 83%, respectively. SEM and AFM observations showed micro-sized and needle-like morphologies for P-CMFs and P-CNCs with an average diameter of 15 μm and 20.5 nm, respectively. The thermal properties of P-CMFs indicate early dehydration with high char formation, while the high thermal stability of P-CNCs (T_{max} = 352 °C) was similar to that of microcrystalline cellulose. The present work showed new routes for preparing phosphorylated micro- and nano-cellulose from a new natural source, having new functions that benefit various applications.

A. Ait Benhamou · M. Nadifiyine
Materials Science and Process Optimization Laboratory, Faculty of science Semlalia, Cadi Ayyad University, 40000 Marrakech, Morocco

A. Ait Benhamou · A. Moubarik
Chemical Processes and Applied Materials Laboratory, Polydisciplinary Faculty, Sultan Moulay Slimane University, BP 592, Beni-Mellal, Morocco

Z. Kassab (✉) · M. H. Salim · H. Sehaqui · M. El Achaby (✉)
Materials Science, Energy and Nanoengineering (MSN) Department, Mohammed VI Polytechnic University, Lot 660 – Hay Moulay Rachid, 43150 Benguerir, Morocco
e-mail: zineb.kassab@um6p.ma

M. El Achaby
e-mail: mounir.elachaby@um6p.ma

Graphic abstract

Giant reed Cellulose
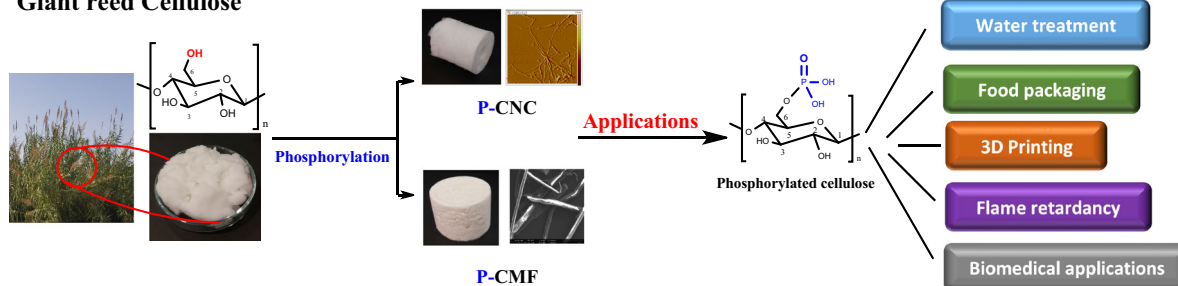
Introduction

It is well-known that cellulose is the most abundant renewable biopolymer on earth derived from biomass, with an estimated production of about $10^{11}-10^{12}$ tons per year (Kadimi et al. 2016). Owing to its unique properties, such as biodegradability, low density, and good mechanical properties, about 6×10^9 tons are used as a raw material in many applications including, textiles and papermaking (Lavoine et al. 2012; Bahloul et al. 2020). In nature, cellulose production can be involved in two separate pathways, either by natural synthesis (photosynthesis procedures) or by bacterial synthesis (Illy et al. 2015; Trache et al. 2017). Cellulose is present in numerous plants, marine biomass/animals, fungi, and bacteria; the primary source of cellulose is wood (Trache et al. 2017), e.g., 10 g of cellulose per day can be produced by a tree (Dufresne 2019).

Nowadays, attention has turned towards nanocellulose as a promising renewable bio-nanomaterial (Noguchi et al. 2017; Rol et al. 2019; Trache et al. 2020a), showing excellent attractive properties such as high strength, high crystallinity, high specific surface area, high aspect ratio, high stiffness, low thermal expansion coefficient, excellent chemical and colloidal stability (Noguchi et al. 2017; Tarchoun et al. 2019b; Kassab et al. 2020b). These properties make nanocellulose a viable source in various applications (Tian and He 2016; Liao et al. 2019; Trache et al. 2020a). Cellulose can be processed into micro-structured materials (cellulose microfibrils (CMFs), and cellulose microcrystals (MCCs)) and nanomaterials (cellulose nanocrystals (CNCs), cellulose nanofibrils (CNFs), and bacterial nanocellulose) using combined effects of chemical and mechanical treatments (Trache et al. 2017, 2020a; Rol et al. 2019; Bahloul et al. 2020). CNCs are an exciting class of nanomaterials due to their natural origin and inherent properties (Kassab et al. 2019b; Trache et al. 2020a, b). CNCs have mainly been used as low-cost sustainable materials in different fields, including packaging, fire retardancy, 3D printing, heavy metal adsorption, and biomedical applications (Liu et al. 2015; Siqueira et al. 2017; Trache 2018; Athukoralalage et al. 2019; Fiss et al. 2019; Mahmud et al. 2019; Rol et al. 2019; Lehtonen et al. 2020; Trache et al. 2020a).

Currently, several studies have focused on improving cellulosic material properties via chemical functionalization as a pretreatment to graft functional groups on their surfaces, giving them enhanced performances that expand their use in specific fields of applications (Ghanadpour et al. 2015; Tian and He 2016; Noguchi et al. 2017; Rol et al. 2019). The main challenge of these protocols is related to the use of toxic compounds with complex protocols, which is still quite challenging at the industrial level (Isik et al. 2014; Rol et al. 2020). Phosphorylation is considered a promising green alternative method to these modifications, using water as a green solvent (Noguchi et al. 2017; Rol et al. 2019). It also leads to the formation of anionic groups on the surface of cellulose, with an important charge content (CC) reaching more than 4000 mmol kg^{-1} (mmol of negative charges per kilogram of cellulose) (Rol et al. 2020).

The application of phosphate derivative compounds in combination with cellulose materials is an old process that has been developed in numerous studies since 1930 using different organic solvents in combination with several phosphorous agents (Reid et al. 1949; Granja et al. 2001; Suflet et al. 2006; Aoki and Nishio 2010; Illy et al. 2015). Currently, limited studies report more convenient cellulose phosphorylation using water as a green solvent. Ghanadpour et al. developed a new phosphorylation protocol, using $(NH_4)_2HPO_4$ in the presence of urea with a curing temperature of 150 °C for 1 h (Ghanadpour et al. 2015). The resulting phosphorylated CNFs exhibited a maximum CC of 1800 mmol kg^{-1}. Later, Noguchi et al. used another phosphorylation process, where softwood pulp sheets were soaked in a solution of $NH_4H_2PO_4$/urea, dried, and then cured in hot temperature at 165 °C for 10 min (Noguchi et al. 2017). The obtained P-CNFs showed higher CC (2200 mmol kg^{-1}). More recently, Rol et al. optimized, for the first time, the phosphorylation protocol adopted from Ghanadpour et al. using different phosphate salts to improve phosphorylation efficiency (Rol et al. 2020). The prepared samples showed a significant increase in the final CC reaching 4400 mmol kg^{-1}. Whereas without urea, phosphorylation occurs with a small amount of CC as previously reported in the literature (Camarero Espinosa et al. 2013; Kokol et al. 2015; Baek et al. 2018).

In this work, Giant Reed (GR) plant was used among all renewable materials to produce phosphorylated cellulose, aiming to valorize unexplored Moroccan resources. Giant Reed, also known as *Arundo Donax L*, is an herbaceous plant belonging to the *Poaceae* family (Fernando et al. 2016). It is of Asian origins (Silva et al. 2014), generally found growing spontaneously in all countries overlooking the Mediterranean Sea (Fernando et al. 2016), particularly Morocco. Generally, its average productivity of dry matter can reach 3 to 37 t/ha, which is slightly higher than that of sugar cane (5 to 23 t/ha) (Silva et al. 2014). Moreover, GR grows in warm and hot climates, especially in wet places, including rivers, lakes, and irrigation canals (Jiao et al. 2016; Tarchoun et al. 2019a). This non-woody material is considered a promising material for energy production due to its rapid growth rate, high capability to adapt to different climate conditions as well as resistance to long arid season (Silva et al. 2014). For several decades, GR was

mainly used in traditional applications such as musical instruments (woodwind), paper making, hand-woven baskets, fishing roars, etc. (Lewandowski et al. 2003; Fiore et al. 2014). Recently, few studies investigate cellulose production and GR application due to its significant cellulose content (49.4–33%) (Barana et al. 2016; Jiao et al. 2016; Tarchoun et al. 2019a; Bessa et al. 2021).

The novelty of this work is the processing of extracted cellulose from GR to phosphorylated micro- and nano- cellulose. The application of $NH_4H_2PO_4$ in a water-based urea system at high temperature leads to the formation of phosphorylated cellulose microfibers (P-CMFs) with high CC, important char formation as well as early thermal degradation. At the same time, the use of only phosphoric acid revealed the formation of phosphorylated-CNCs with low CC, high crystallinity, and thermal stability. The phosphorylated cellulose (P-CMFs, and P-CNCs) were studied in terms of their CC, chemical structure, crystallinity, morphologies, and thermal stability.

Materials and methods

Chemicals and raw material

Giant reed (*Arundo donax*) plant (Fig. 1), were collected from a local farm in Beni-Mellal-Khenifra region, Morocco. Microcrystalline cellulose powder (MCC) was obtained from Alfa Aesar. Phosphoric acid (H_3PO_4, 85%), sodium hydroxide (NaOH, > 97%), glacial acetic acid (CH_3COOH, > 99%), sodium chlorite ($NaClO_2$, 80%), Urea (($NH_2)_2CO$) and Ammonium dihydrogen phosphate (ADP) ($NH_4H_2PO_4$), were purchased from Sigma Aldrich. All chemicals were used as received without further modification.

Extraction of cellulose microfibers

As reported in previous works (Bahloul et al. 2020; Kassab et al. 2020a, c; Boussetta et al. 2021), cellulose microfibers (CMFs) extraction has been done in three steps. Firstly, crushed raw Giant Reed (GR) (1.5 mm) were treated in distilled water for 1 h at 60 °C in order to eliminate organic and hot water extractives (Beroual et al. 2021). The solid-to-liquid ratio used was 1:20 (g:mL). At the end of the treatment, the pre-
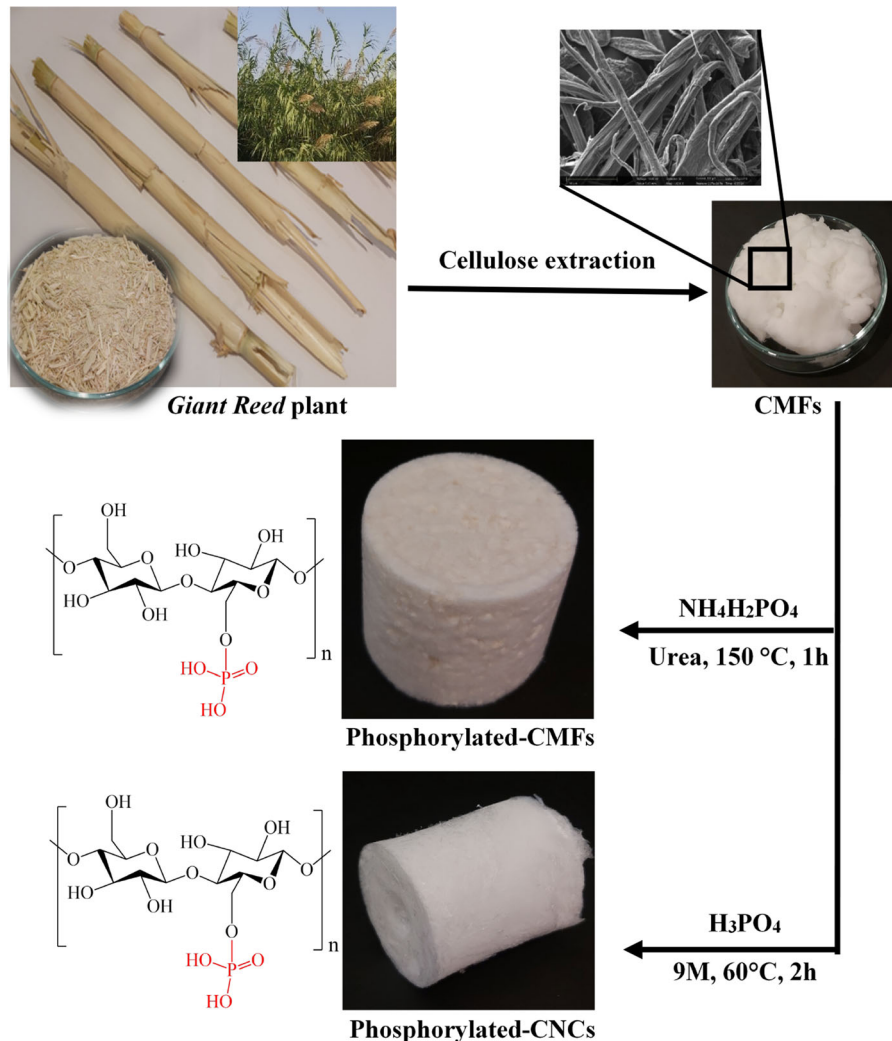
Fig. 1 Overall steps for P-CMFs and P-CNCs extractions using two different phosphorylation processes of CMFs from raw GR

treated *GR* was cooled and washed with distilled water to remove the solubilized compounds and organic extractives. Afterward, the GR residue was treated three times with an aqueous alkaline solution (4 wt.% NaOH (m/v) at 80 °C for 2 h under stirring. The residue was washed with water until achieving a neutral pH. Finally, the alkali-treated fibers were successively bleached using a bleaching solution made up of equal parts (v:v) of acetate buffer (27 g NaOH and 75 mL glacial acetic acid, diluted to 1 L of distilled water) and aqueous sodium chlorite (1.7 wt.% NaClO$_2$ in water). This treatment was done three times, resulting in pure cellulose microfibers (Fig. 1).

Phosphorylation of cellulose microfibers

Phosphorylated cellulose microfibers from GR plant were successfully prepared using the well-known phosphorylation process in the presence of urea, according to previous works in literature (Ghanadpour et al. 2015; Noguchi et al. 2017). For that, 4.5 g of ADP (NH$_4$H$_2$PO$_4$) and 12 g of urea were solubilized under stirring in 15 g of deionized water. After that, the prepared solution was added dropwise to 10 g of dispersed CMFs evenly. Then, wet CMFs were dried overnight at 60 °C, and cured for 1 h in hot temperature (150 °C). Finally, the phosphorylated fibers were cooled and repeatedly washed with distilled water to remove non-attached reagents. The resulting product

was denoted phosphorylated cellulose microfibers (P-CMFs) (see Fig. 1).

Preparation of phosphorylated P-CNCs

Phosphorylated cellulose nanocrystals (P-CNCs) were isolated using phosphoric acid hydrolysis (Camarero Espinosa et al. 2013; Zhang et al. 2014; Kassab et al. 2020c). 1 g of CMFs was added to 20 ml of preheated phosphoric acid (9 M) in reflux heating at 60 °C. The mixture was repeatedly homogenized for 2 h by mechanical stirring. Afterward, the obtained mixture was cooled in an ice bath to stop the reaction. The diluted mixture was then washed by successive centrifugation at 12,000 rpm for 20 min at 15 °C to remove the remaining acids. The resulting CNC suspension was exposed to dialysis against distilled water for 4-6 days until a constant neutral pH was reached. The resulted P-CNCs (Fig. 1) were consequently sonicated in an ice bath for 5 min using an ultrasonic homogenizer at 25% amplitude, and a partial quantity of suspension was freeze-dried and stored for further characterizations.

Conductometric titration

The charge content (CC) of phosphorylated cellulose samples was determined using modified conductometric titration process from previous works (Camarero Espinosa et al. 2013; Ghanadpour et al. 2015; Kokol et al. 2015; Noguchi et al. 2017). For that, 0.3 g of phosphorylated samples (P-CMFs and P-CNCs) were dispersed in distilled water (100 mL) containing 10 mL of NaCl (0.01 M), and the mixture was homogenized for 5 min in an ice bath.

The pH of the mixture was reduced to the range 2.5–3 using hydrochloric acid (0.1 M). After that, NaOH (0.1 M) solution was added stepwise while the conductivity was monitored. This was continued until the pH reached 11. The CC was determined using the following Eq. (1):

$$CC\,(mmol\,kg^{-1}) = \frac{C_{NaOH} \times V_{NaOH}}{W_{CNC}} \times 10^6 \qquad (1)$$

where V_{NaOH} is the added volume (L) corresponding to the plateau length, C_{NaOH} is the employed concentration of NaOH (M), and W_{CNC} is the used weight of phosphorylated samples (g) (Camarero Espinosa et al. 2013).

Characterization

The chemical structure of the cellulosic materials was studied using Fourier transform infrared spectroscopy (FTIR, Perkin-Elmer Spectrum 2000) equipped with ATR accessory. All FTIR spectra were recorded in 4000–600 cm^{-1} range with a resolution of 4 cm^{-1} and an accumulation of 16 scans. The crystalline structure of all studied cellulosic materials was determined using X-Ray diffractometer (D2 PHASER diffractometer, BRUKER). Each material was prepared in the form of powder then placed on the sample holder to obtain uniform X-ray exposure. The samples were scanned with CuK radiation (λ = 1.54056 Å) in the 2 range of 5–40 °C, while the voltage and current were fixed at 40 kV and 40 mA, respectively. To study the crystallinity of all cellulosic materials, the crystallinity index (CrI) was calculated following the equation of Segal (2) (Segal et al. 1958):

$$CrI = \frac{I_{200} - I_{am}}{I_{200}} \times 100 \qquad (2)$$

where I_{200} is the maximum intensity of the (200)-lattice peak at around $2\theta = 22.8°$, and I_{am} is the intensity from the amorphous phase at approximately $2\theta = 18.6°$.

The effect of chemical treatment on cellulose microfibers morphologies and fibers diameter was examined using a scanning electron microscope (SEM, Zeiss Evo 10) operated at 15 kV. For that, the samples were coated with a thin conductive carbon layer using an ion sputtering apparatus. Atomic force microscopy (AFM, Veeco Dimension ICON) was used to investigate the morphology and dimensions of the nanocrystals. Samples were prepared as follows, 0.01 wt% of CNCs dispersed in aqueous solution was sonicated for 5 min, then deposited on a mica sheet, and dried in an oven at 80 °C for 15 min. The analysis was performed in tapping mode and image treatments were carried out using Veeco Data Analysis Software.

The thermal stability and the degradation behavior of all samples were evaluated by thermogravimetric analysis (TGA) using TA instruments (Discovery TGA,). Samples were heated from room temperature to 700 °C at a heating rate of 10 °C/min. All measurements were done under a nitrogen atmosphere with a gas flow of 20 mL min^{-1} to prevent oxidation effects.

Results and discussions

Possible chemical structure of phosphorylated cellulose fibers

Commonly, cellulose phosphorylation creates functional groups on the surface of fibers via substitution of the free hydroxyl groups present in C2, C3, or C6 sites by phosphoric groups (Aoki and Nishio 2010; Kokol et al. 2015). As a result, different uncrosslinked and crosslinked structures are produced, as shown in Fig. 2.

Regarding the uncrosslinked structures, phosphoric acid or phosphate salts react with the free hydroxyl of cellulose forming phosphate groups with two acidic protons (Cell-O-P(O)(OH)$_2$) or phosphite groups with one acidic proton (Cell-O-P(H)(=O)(OH)), as depicted in Fig. 2 (form A-1 and B-1) (Kokol et al. 2015; Rol et al. 2020). While, crosslinking structures can also occur due to the presence of high CC (Noguchi et al. 2017), where the possibility of crosslinking with one or two strong acids appear (see depicted form 2 and 3). Another possibility of crosslinking structure can also be found with tri-substituted esters (form 4) (Kokol et al. 2015). Furthermore, the presence of some aggregates in phosphorylated samples is a clear indication that confirms the presence of crosslinked structures, as reported by Rol et al. (2020). These aggregates are tough to destroy and are undesirable in

the process of nano-fibrillation (Rol et al. 2019). Otherwise, without urea, phosphorylation also leads to the structures mentioned above (form A-1 and B-1 in Fig. 2), with no crosslinking structures due to the presence of low CC (Kokol et al. 2015). Besides, conductometric titration, FTIR, and TGA analyses could be used to determine fiber's possible structures and phosphate position.

Phosphate content measurement

Conductometric titration was performed as an efficient method to measure the CC and get more information about the possible phosphorus form created. It was previously reported that the conductometric titration could help in investigating the possible chemical structure of phosphorylated cellulose (Suflet et al. 2006; Kokol et al. 2015). Figure 3a, b show the conductometric titration curves of P-CNCs and P-CMFs, respectively.

Generally, conductivity curves with strong acid and base can be divided into three specific regions (Kawaguchi et al. 1995; Dos Santos et al. 2009). The first region corresponds to the consumption of strong free protons H$^+$ present in solution, which leads to an important decrease in conductivity due to the NaOH addition. The second region is related to the neutralization of weak acids present in the surface of

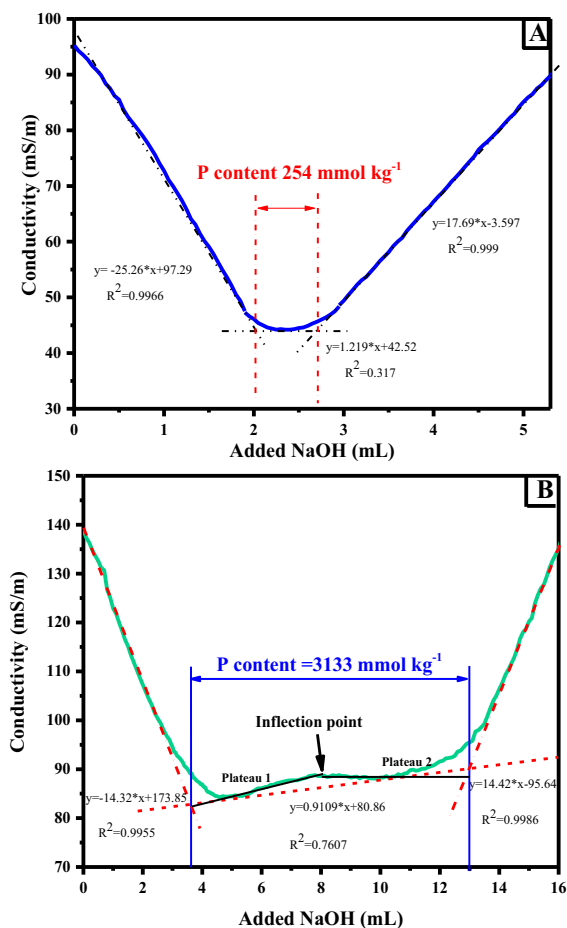**Fig. 2** Possible phosphorylated cellulose structure
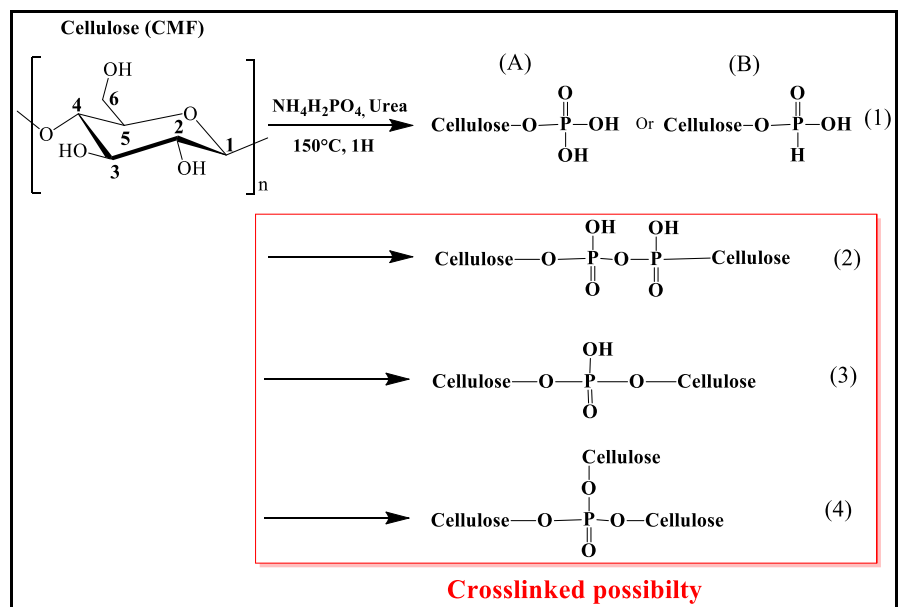
Fig. 3 Conductometric titration curves of **a** P-CNCs and **b** P-CMFs

cellulose, and the final region is assigned to the excess of added NaOH.

In the case of P-CNCs, the conductometric titration curve (Fig. 3a) clearly indicates the presence of only one inflection point, which divided the curve into three major regions, as already seen. The presence of one plateau means that only one -OH group was titrated by this method, similarly as reported by Espinosa et al. (Camarero Espinosa et al. 2013). While the P-CMFs curve (Fig. 3b) exhibited an additional plateau due to the presence of three inflection points, indicating that two hydroxyl groups have been consumed during the titration process. Moreover, it is also clear from the titration curves that the total CC increased with increasing plateau length, and P-CMFs exhibited a longer plateau than that observed for P-CNCs, which explains the high measured CC for P-CMFs 3133

mmol kg^{-1} compared to P-CNCs 254 mmol kg^{-1}. This high difference in CC was expected since the phosphorylation without urea leads to a very low CC on the surface of cellulose, as previously reported in the literature (Camarero Espinosa et al. 2013; Kokol et al. 2015; Baek et al. 2018; Kassab et al. 2020c). While the presence of urea in phosphorylation allows obtaining a large amount of phosphate as in the case of molten urea (Kokol et al. 2015), or in the case of a water-based urea system, which is in accordance with the results obtained (Ghanadpour et al. 2015; Noguchi et al. 2017; Rol et al. 2020).

Regarding the possible chemical structure, the titration of two hydroxyl groups with high CC in the surface of P-CMFs indicates clearly that the chemical structure exhibited phosphate groups (Cell-O-P(O)(OH)$_2$) with two acids (see depicted form A-1 in Fig. 2). This aspect was in total agreement with FTIR analysis that showed the absence of P-H peak at about 2360 cm^{-1} in P-CMF sample (see below). While the presence of only one plateau is not sufficient to predict the chemical structure of attached phosphorous to CNC due to the low CC as well as the absence of characteristic peaks (P–O–C; P–OH and P–H) in FTIR spectra (Fig. 4).

FTIR analysis

FTIR analysis is an efficient method to assess the structural changes that occurred during different stages of treatments and to confirm the functional groups present in the P-CMFs and P-CNCs (Kassab et al. 2020c).

Figure 4a shows a comparison between FTIR spectra obtained for raw GR, extracted CMFs, and MCC. It can be seen that the characteristic bands of cellulose molecules were observed in all the samples, which are comparable to the commercial MCC (Tarchoun et al. 2019a; Kassab et al. 2020c), and cellulose from other sources (Bahloul et al. 2020; Kassab et al. 2020a, c). Commonly, the broadband at 3335 cm^{-1} correspond to O–H stretching vibrations, the peak at 2903 cm^{-1} are assigned to C–H stretching vibrations of CH$_2$ group and the band around 1628 cm^{-1} is due to deformation vibration of absorbed water, related to the hydrophilic nature of cellulosic materials (Liu et al. 2015; Tarchoun et al. 2019a; Kassab et al. 2020c; Ait Benhamou et al. 2021). Besides, the three bands that appeared at
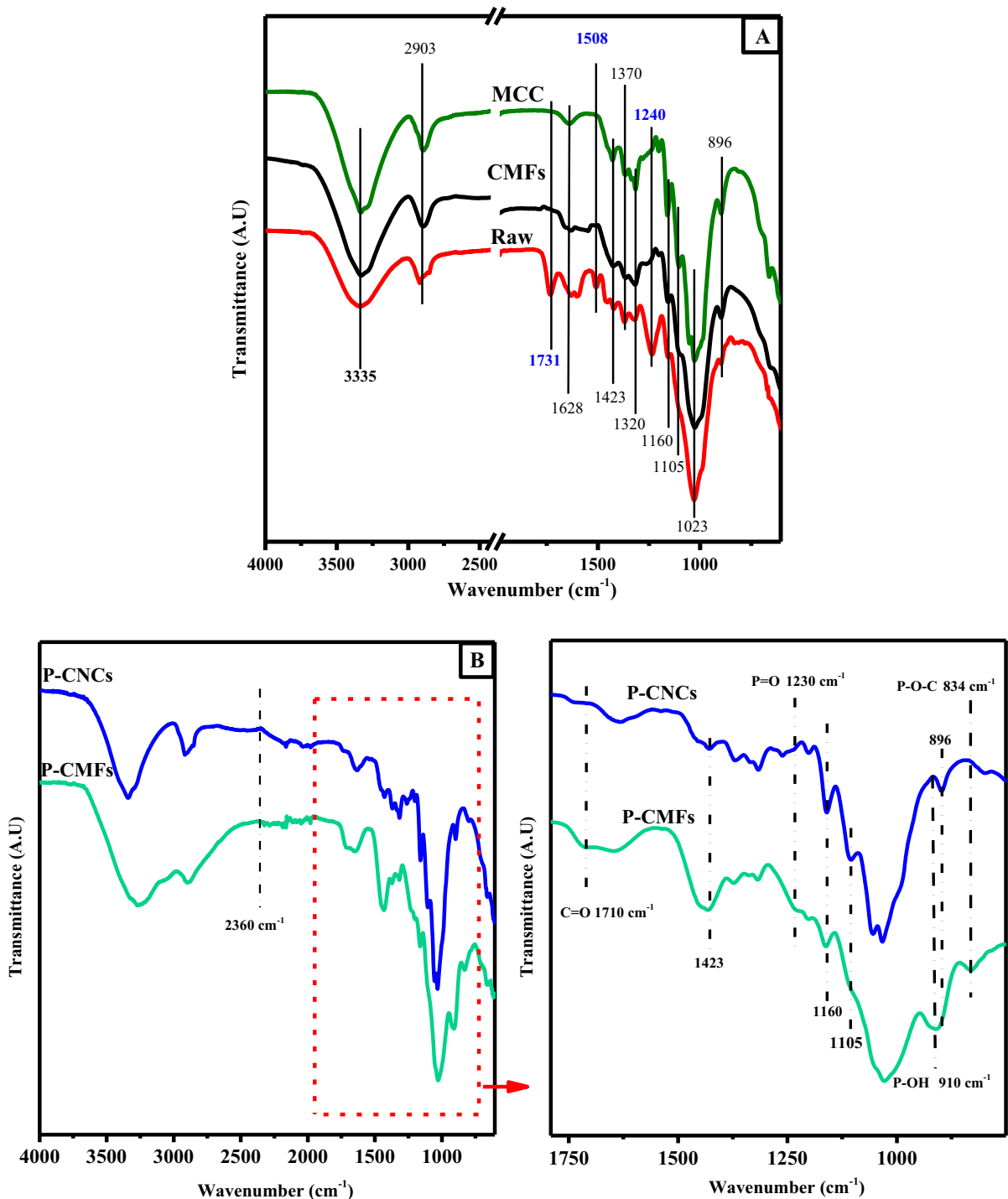
Fig. 4 FTIR spectra of raw GR, extracted CMFs, and MCC (**a**) and P-CMFs with P-CNCs samples (**b**)

1423 cm^{-1}, 1370 cm^{-1}, and 1320 cm^{-1} are attributed to CH$_2$ symmetric bending vibration, C–O symmetric stretching, or C-H asymmetric deformation in

polysaccharide aromatic rings of cellulose and C–H bending, respectively (Tarchoun et al. 2019a; Kassab et al. 2020c). Furthermore, the bands located at

1160 cm^{-1}, 1105 cm^{-1}, 1023 cm^{-1}, and 896 cm^{-1} are related to C–O–C asymmetric bridge vibration of the b-glycosidic linkage, C–O pyranose ring skeletal stretching, C–O bond stretching, and C$_1$–H deformation with ring vibration contribution and OH bending, respectively (Tarchoun et al. 2019a; Kassab et al. 2020c).

From Fig. 4a, it is clear that raw GR shows some changes compared to the spectrum of the extracted CMFs and commercial MCC due to the elimination of non-cellulosic components (Kassab et al. 2020c). The bands at 1733 cm^{-1}, 1508 cm^{-1}, and 1240 cm^{-1} observed only in raw GR sample are assigned to C=O stretching vibration of the carbonyl and acetyl groups in the xylan component of hemicelluloses or the ester linkage of the carboxylic group of ferulic and p-coumaric acids of lignin and/or hemicelluloses, the C = C stretching vibrations from the aromatic hydrocarbons in lignin and C–O out-of-plane-stretching-vibration of the aryl group of lignin and hemicelluloses molecules (Tarchoun et al. 2019a; Kassab et al. 2020c). In contrast, these peaks are not detected in the spectrums of CMFs, P-CMFs, and P-CNCs, which clearly indicates that the treatment results in the total elimination of non-cellulosic components. To the best of our knowledge, the presence of bands at 1423 cm^{-1}, 1160 cm^{-1}, 1105 cm^{-1} and 896 cm^{-1} in the CMFs spectrum indicates clearly that the extracted CMFs from GR plant are in the form of cellulose I structure (Fortunati et al. 2013; Kassab et al. 2020c), which is in accordance with XRD analysis (Fig. 5).

Figure 4b compiles FTIR spectra of phosphorylated cellulose P-CMFs and P-CNCs. As shown, additional new peaks were detected at 834 cm^{-1} and 910 cm^{-1}, generally corresponding to P–O–C aliphatic bond and P–OH stretching mode, respectively (Ghanadpour et al. 2015; Lehtonen et al. 2020). Also, the presence of a new slight band at 1230 cm^{-1} assigned to the P=O stretching vibration supports the phosphorylation of cellulose (Ghanadpour et al. 2015; Lehtonen et al. 2020). The presence of a new sharp band at 1710 cm^{-1} corresponded to C=O stretching vibration indicates that partial oxidation of cellulose occurs during the reaction (Aoki and Nishio 2010; Ghanadpour et al. 2015).

In contrast, the two bonds relative to P–O–C and P–OH vibrations were not detected for the P-CNCs. While the intensity of P=O band was inferior for P-CNCs than that in P-CMFs which is probably related to the applied phosphorylation process without urea that graft low content of phosphate groups in the surface of nanocrystals as observed in conductometric titration (254 mmol kg^{-1} for P-CNCs compared to 3133 mmol kg^{-1} for P-CMFs). Similar findings were reported previously using the same protocol (Camarero Espinosa et al. 2013; Kassab et al. 2020c). Moreover, the absence of P-H bond adsorption (2360 cm^{-1}), and the presence of P=O and P–OH bonds in P-CMFs, indicates that the attached phosphorous to cellulose was in the form of phosphate groups containing two acidic protons (Ghanadpour et al. 2015; Kokol et al. 2015; Noguchi et al. 2017), which confirms the structure depicted in Fig. 2 (form A-1). While for P-CNCs, it is not evident to predict its structure due to the low CC that influences the presence of characteristic peaks in FTIR spectra, which strengthens the presence of two proposed possibilities except for crosslinked one. These results confirm the conductometric titration findings.

X-ray diffraction

XRD analysis was used to study the crystalline structure and the crystallinity index of all studied samples (GR, CMFs, P-CMFs, and P-CNCs). Figure 5 shows the XRD patterns of all samples and the determined crystallinity index is mentioned in Table 1. It is clear that all samples exhibited four major peaks at 2θ = 14.9, 16.7, 22.5, and 34.6 attributed to the crystallographic planes of 1$\bar{1}$0, 110, 200, and 004, respectively, all of which were in accordance with typical reflection planes of cellulose I structure (Tang et al. 2015; Gong et al. 2017). These results clearly indicate that there are no changes in the polymorphism of cellulose I after different consecutive treatments, including bleaching treatments and phosphorylation processes, which confirms that GR plant could be categorized as a lignocellulosic material.

The measured crystallinity index of raw GR was 56%, while that of extracted CMFs was 73% (Table 1). This improvement in CrI from raw to extracted cellulose can be explained by the total elimination of amorphous non-cellulosic components (Hemicellulose, lignin, pectin and wax) by alkali and bleaching treatments (Fujisawa et al. 2014), as
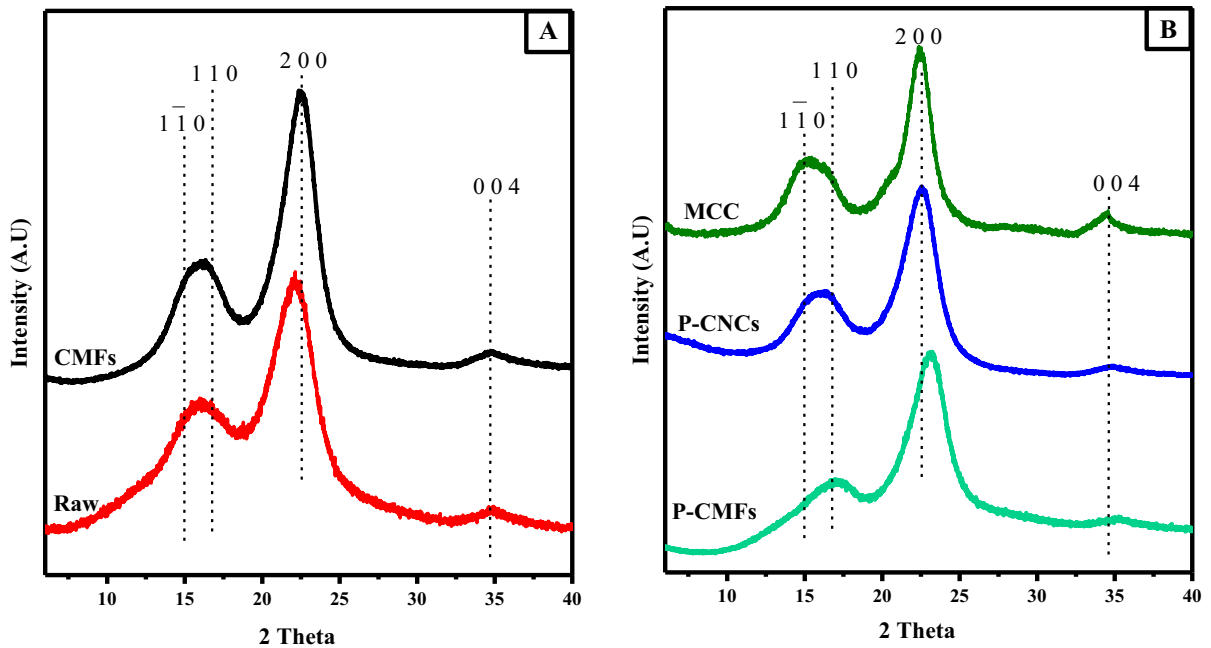
Fig. 5 XRD patterns of raw GR fibers and extracted CMFs (**a**), P-CMFs, P-CNCs and MCC

Table 1 Structural, morphological and thermal parameters of GR fibers, CMFs, P-CMFs, P-CNCs and MCC samples

Samples	Crystallinity index%	SEM or AFM		TGA/DTG			Charge content (mmolkg^{-1})
		D (μm ornm)	L (nm)	$T_{onset10\%}$ (°C)	T_{max} (°C)	R (%) at 600 °C	
Raw	56	115 μm ± 3.4	–	230	318	25	–
CMFs	73	13 μm ± 1.2	–	261	330	23	–
P-CMFs	70	15 μm ± 2.3	–	217	257	50	3133
P-CNCs	83	20.5 nm ± 2.6	674 ± 152	294	352	22	254
MCC	83	–	–	301	326	5	–

confirmed by FTIR analysis. This finding is close to that reported for CMF extraction from a similar source using another isolation process (CrI = 54 and 68% for raw and CMFs, respectively) (Tarchoun et al. 2019a).

The crystallinity of phosphorylated samples depends strongly on the type of phosphorylation (Fig. 5; Table 1). The obtained CrI values were found to be 70%, 83 and 83% for P-CMFs, P-CNCs and MCC, respectively. This slight reduction of about 3% in the crystallinity index of P-CMFs compared to purified CMFs related to the presence of a large amount of phosphate groups (3133 mmol kg^{-1}) in the amorphous part of cellulose. As commonly known,

cellulose phosphorylation generally occurs in the amorphous regions (Kokol et al. 2015).

On the other hand, the obtained CrI of P-CNCs is higher than that of CMFs and compared to that obtained for MCC (83%). This finding indicates that acid hydrolysis increased the crystallinity of the resultant P-CNCs, due to the role of applied acid that attacks the amorphous domains of the extracted CMFs and leaves the crystalline one unaltered, as seen in AFM image (Fig. 7). Similar findings were reported previously using the same method to extract P-CNCs from other sources such as tomato plant residue (Kassab et al. 2020c), and Whatman filter paper

(Camarero Espinosa et al. 2013). Whereas, lower CrI was reported for P-CNCs extracted from bamboo source 67% (Zhang et al. 2014), and for P-CNCs from medical cotton 58% (Mahmud et al. 2019).

Morphological characterization

Scanning electron micrographs of raw GR fibers, extracted CMFs and P-CMFs were shown in Fig. 6. These micrographs were recorded to explore the morphological features after different chemical treatments and to determine the dimensions of all studied samples.

The SEM micrographs of raw GR (Fig. 6a) indicate the presence of long fibers with hierarchical structure and rough surface, as reported previously (Zhang et al. 2014; Tarchoun et al. 2019a). This roughness indicates that the cell walls of raw GR fibers have a compact structure, where cellulose fibers are immersed in an open matrix of hemicellulose and lignin (Giudicianni et al. 2014; Kassab et al. 2019c). In Fig. 6b, individual clean fibers with thinner and shorter dimensions were observed for purified CMFs. Using alkali treatment,

the non-cellulosic compounds (lignin and hemicellulose) were partially removed from the raw GR fibers (Kassab et al. 2019c). After the bleaching treatment, the total removal of the cementing materials resulting in defibrillated microfibers.

The average diameter of raw GR fibers was considerably decreased from 115 to 13 μm (Table 1) after successive chemical treatments. This finding is in accordance with previous studies (Kassab et al. 2019c, 2020a, c), using the same protocol to purify cellulose microfibers, resulting in the total elimination of non-cellulosic components as confirmed in FTIR analysis (Fig. 4). Furthermore, the obtained yield of the CMFs from the initial dry weight of GR was found to be 36%. It is essential to know that the obtained yield is similar to that extracted from the same plant, using another bleaching treatment (Tarchoun et al. 2019a). In comparison to CMFs isolated from other bio-sourced materials using the same bleaching treatment, the obtained yield is quite comparable to that extracted from tomato plant residue (37%) (Kassab et al. 2020c), and Alfa fibers (40%) (Kassab et al. 2019c).
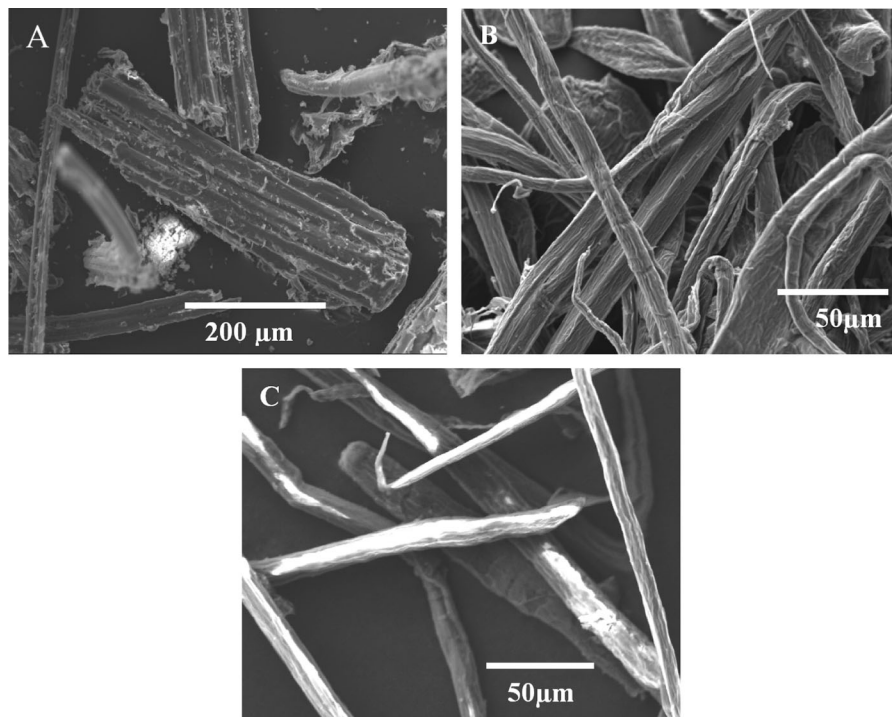

Fig. 6 SEM images of Raw GR (**a**), as-extracted CMFs (**b**), and P-CMFs (**c**)

After cellulose phosphorylation, the fibrillation of microfibers was not altered as shown in P-CMFs micrograph (Fig. 6c). Where, the average diameter was found to be in the range of 15 μm ± 2.3, which is quite comparable to that measured for pure CMFs (13 μm ± 1.2). Thus, confirming the stability of CMFs after partial oxidation during curing at high temperature, as seen in FTIR analysis.

To study the successful extraction of P-CNCs from giant reed CMFs, the morphology and dimensions of P-CNCs were investigated based on AFM micrographs (Fig. 7). The diameter and length were measured using Image J as a digital image analyzer (Kassab et al. 2019a), and the obtained results are summarized in Table 1.

After the phosphoric acid attack, the amorphous regions of the isolated CMFs were hydrolyzed. Simultaneously, the crystalline one shows higher stability and resistivity against harsh acid attack, resulting in P-CNCs extraction (Fig. 7). It is clear that P-CNCs exhibit a needle-like morphology with an irregular size distribution, confirming their successful extraction from giant reed CMFs. Moreover, the needle-like shape is the most acquired morphology for CNCs after different acid hydrolysis processes (Zhang et al. 2014; Cheng et al. 2020; Kassab et al. 2020b). This finding confirms the observed increase in CrI (Table 1) of P-CNCs compared to CMFs one.

Otherwise, the P-CNCs extracted from other sources using phosphoric acid hydrolysis leads to

P-CNCs with different dimensions. Herein, the average diameter (D) and length (L) of P-CNCs are 20.5 ± 2.6 nm and 674 ± 152 nm, respectively, while that measured for P-CNCs extracted from Whatman filter paper and tomato plant residue are (D = 31 ± 14 nm, L = 316 ± 127 nm) (Camarero Espinosa et al. 2013), and (D = 6.2 ± 2.4 nm L = 610 ± 115 nm) (Kassab et al. 2020c), respectively. This is probably attributed to the original nature of the cellulose extracted from different sources, leading to different dimensions, according to our previous work (Kassab et al. 2020c). Not only that, but it is also reported that the isolation conditions play an important role in the resulting CNC dimensions (Cudjoe et al. 2017).

Regarding the aspect ratio (L/D), it is worthwhile noting that the CNC aspect ratio is one of the most decisive parameters to assess their usefulness as reinforcements materials (Kassab et al. 2020c). Therefore, it was reported in the literature that CNCs with high (L/D) shows high tensile strength compared to carbon fibers, Kevlar and stainless steel (Cudjoe et al. 2017). This property makes CNCs promising candidates for nanocomposites development (Fortunati et al. 2013; Cudjoe et al. 2017).

In this study, the aspect ratio was found to be (L/D) = 33 for P-CNCs from giant reed, which is higher than that of P-CNCs from Whatman filter paper (L/D) = 11 (Camarero Espinosa et al. 2013), and lower than that of P-CNCs from tomato plant residue (L/D) = 98 (Kassab et al. 2020c). It is observed that phosphoric
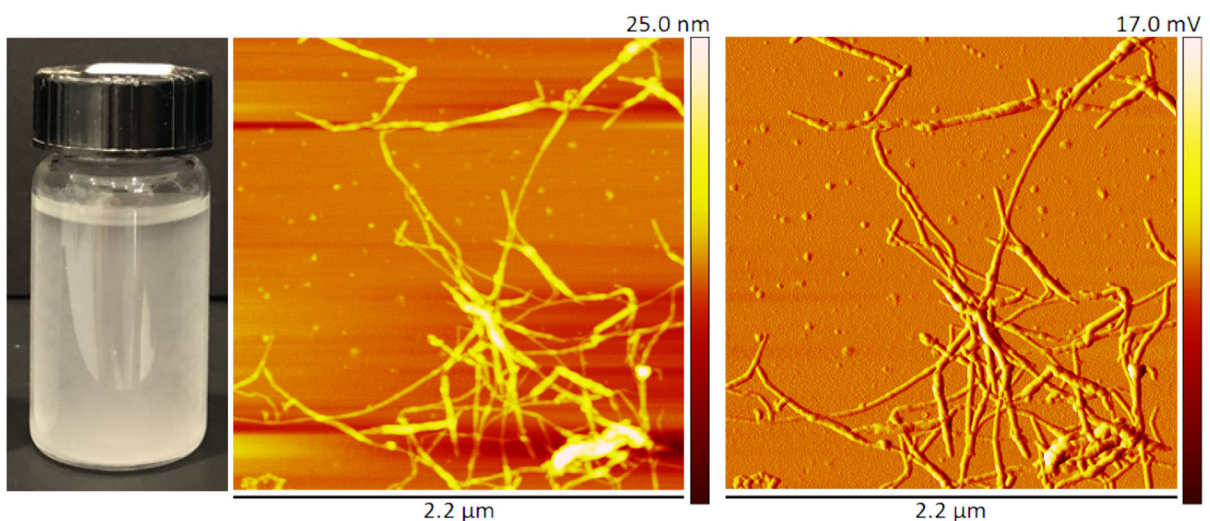

Fig. 7 Aqueous suspension and AFM images of P-CNCs

acid hydrolysis produces P-CNCs with promising reinforcement effects, taking into consideration that the minimum value of aspect ratio acquired for a good stress transfer from the polymer to the nanofibers for any significant reinforcement to occur is (L/D) = 10 (Flauzino Neto et al. 2013).

Thermal analysis

The thermal stability of cellulosic materials is a determining factor to assess their suitability as a potential material in different applications, including packaging and flame retardancy (Tarchoun et al. 2019a). The thermal properties of phosphorylated cellulose were investigated by TGA analysis in comparison with pure cellulose and MCC. The TGA/DTG curves of raw GR, CMFs, P-CMFs, P-CNCs and MCC are shown in Fig. 8 and their thermal parameters are listed in Table 1.

It is clear from Fig. 8b that the thermal decomposition of raw GR occurs in several steps, which are related to the decomposition of several compounds such as lignin, cellulose, and hemicellulose that are generally known by their different decomposition temperatures. In contrast, the CMF's DTG curve showed one main loss that corresponds to cellulose decomposition characterized by a single peak centered at 330 °C. Raw GR began to decompose at a temperature range starting from 170 °C and continue up to 360 °C with a maximum decomposition at 318 °C, as seen in the DTG measurement (Fig. 8b).

Moreover, the onset temperature (T_{onset}) of CMFs starts at about 261 °C, which is higher than that observed for raw GR that started at about 230 °C. These results deal with the high thermal stability of CMFs compared to raw GR, due to the total elimination of thermally unstable amorphous compounds (hemicellulose and lignin) after successive chemical treatments (Tarchoun et al. 2019a; Kassab et al. 2020c). This finding was confirmed by the residual mass observed for raw GR (25% at 600 °C), which is slightly higher than that determined for CMFs (23% at 600 °C) owing to the presence of less degradable moisture content in raw GR (8.40%) compared to CMFs (5.22%) (Tarchoun et al. 2019a; Kassab et al. 2020c).

Generally, cellulose decomposition in N_2 atmosphere taking place in one main loss can be presented in two involved steps. At low temperatures, glycosyl units began to decompose into char. In contrast, at higher temperatures, these units depolymerize into volatile products (Ghanadpour et al. 2015). In the case of P-CMFs (Fig. 8b), the T_{onset} and the temperature of maximum degradation (T_{max}) were determined to be 261 °C versus 217 °C and 330 °C versus 257 °C for CMFs and P-CMFs, respectively. These results indicate clearly that P-CMFs exhibited the lowest thermal stability compared to pure CMFs, owing to the phosphate groups that act as a catalyst in promoting early dehydration and char formation resulting in a high reduction of cellulose decomposition (Aoki and Nishio 2010; Camarero Espinosa et al. 2013; Kokol
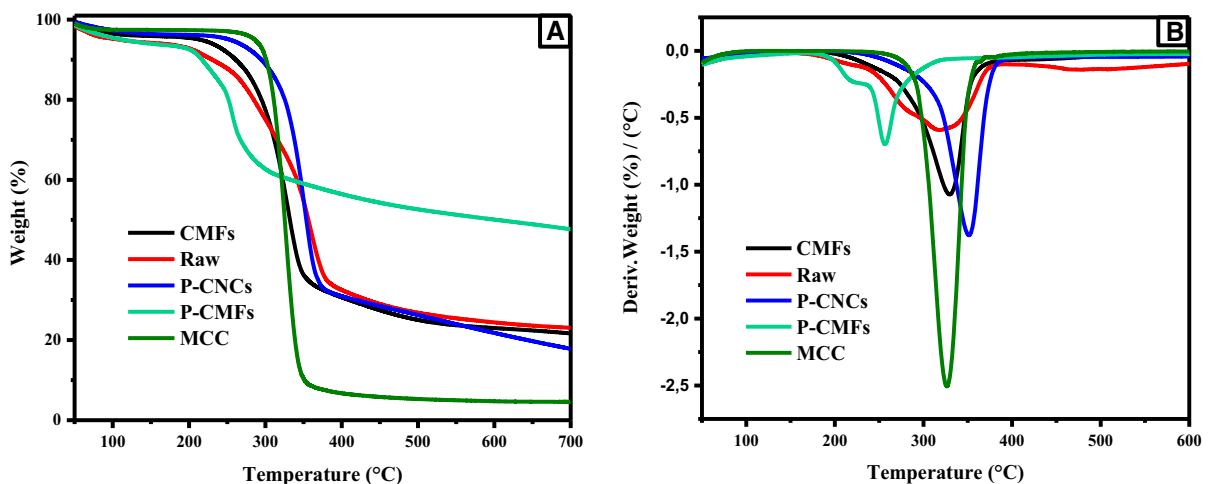

Fig. 8 TGA (a) DTG (b) curves of raw GR fibers, extracted CMFs, P-CMFs and P-CNCs

et al. 2015; Rol et al. 2019). In general, the phosphate groups have been used as flame-retardants due to their capacity of char formation (Aoki and Nishio 2010; Camarero Espinosa et al. 2013), which explains the obtained results of char at 600 °C for P-CMFs (about 50% compared to 23% of raw CMFs). Moreover, the observed increase in P-CMFs residual mass loss indicates clearly that the phosphorylation took place in C6 where the cellulose decomposition was prevented, showing good thermal stability compared to C2 and C3 phosphorylation that leads to better flame resistance effect (Aoki and Nishio 2010; Kokol et al. 2015). These results indicate that P-CMFs could be considered a potential candidate for developing flame-retardant/resistant materials.

On the other hand, the DTG curves of P-CNCs and MCC indicate similar thermal behavior to that of CMFs, with one main loss, showing improved thermal stability compared to extracted CMFs. Regarding the thermal stability, the T_{onset} of P-CNC sample was found to be 294 °C which is comparable to that of MCC (301 °C), while the determined T_{max} was found to be 352 °C for P-CNCs which is higher than that of MCC (326 °C) (Table 1). It was reported previously that the lignocellulosic materials with high thermal stability exhibited high crystallinity index (Kassab et al. 2020c), which is in agreement with our findings. Whereas the TGA curves (Fig. 8a) showed a low char yield for MCC, about 5% at 600 °C, while P-CNCs exhibited 22%. This is due to the effect of functionalization by phosphate groups in the surface of crystals confering a high char yield formation compared to MCC (Camarero Espinosa et al. 2013). This

finding is similar to that reported in the literature using the same phosphorylation process with phosphoric acid (Camarero Espinosa et al. 2013; Zhang et al. 2014; Kassab et al. 2020c).

To investigate the performance of the phosphorylated cellulose and its feasibility in different applications, a comparative study of their thermal stability was performed with other phosphorylated cellulose of previous works in literature. Table 2 displays the thermal parameter as well as their charge density, including the type of phosphorylation process. From Table 2, it is clear that phosphorylated cellulose prepared with urea showed early thermal decomposition, important char formation (about 45–55% at 600 °C), and high CC, starting from 1000 mmol kg^{-1} to more than 3000 mmol kg^{-1}. While, without urea phosphorylated cellulose exhibited low CC, high thermal stability, and low char content. These results can be explained by the important role of urea in phosphorylation that serves as a catalyst, increases the phosphate agent penetration, enhances fibers' swelling, and prevents cellulose decomposition during phosphorylation (Ghanadpour et al. 2015; Rol et al. 2020).

Regarding the thermal stability, it is clear from the onset temperature (T_{onset}), maximum degradation (T_{max}), and char formation that P-CMFs from giant reed showed comparable behavior to phosphorylated samples with urea. As known, phosphate groups act as flame retardants due to their rapid char formation (Ghanadpour et al. 2015), which reflects the early thermal dehydration of phosphorylated cellulose with urea. Moreover, the prepared P-CMFs presented less

Table 2 Thermal stability comparison

Samples	$T_{onset10\%}$ (°C)	T_{max} (°C)	R at 600 °C (%)	Phosphorylation Method	Charge density (mmol kg^{-1})	References
P-CNFs of cellulose sludge	230	–	55	Urea	1173	Kokol et al. (2015)
P-CNFs of commercial sulfite softwood	258	283	40	Urea	1839	Ghanadpour et al. (2015)
P-CMFs of giant reed	217	257	50	Urea	3133	This work
P-CNCs of wood bioethanol residue	225	–	45	Urea	1038	Kokol et al. (2015)
P-CNCs tomato	235	333	21	No urea	79	Kassab et al. (2020c)
P-CNCs filter paper	220	325	12	No urea	10	Camarero Espinosa et al. (2013)
P-CNCs giant reed	294	352	22	No urea	254	This work

T_{onset} and T_{max} (Table 2) than that reported for P-CNFs of commercial sulfite softwood using the same protocol, and that of P-CNFs of cellulose sludge and P-CNCs of wood bioethanol residue using another protocol in molten urea (Table 2). Thus, it indicates the early dehydration of P-CMFs compared to the presented samples. From these results, it is possible to suggest the as-prepared P-CMFs as a green alternative to toxic halogen compounds in developing flame retardant/resistant materials.

Herein, it was also found that the measured CC of P-CMFs (3133 mmol kg^{-1}) is higher than that reported by Ghanadpour et al., (1839 mmol kg^{-1}) using a modified phosphorylation process (Ghanadpour et al. 2015). While in the case of molten urea, low CC was reported by Kokol et al., (1038 and 1173 mmol kg^{-1}) compared to phosphorylated cellulose prepared in water urea system (Kokol et al. 2015). This finding proves that CC could be influenced by several parameters in reaction conditions, including the type of phosphate agent, form of urea (molten or solubilized), reaction time, temperature, and cellulose source.

On the other hand, the onset temperature and maximum degradation of P-CNCs from giant reed were found to be 294 and 352 °C, respectively, which is higher than that of P-CNCs from Whatman filter paper (220–325 °C) (Camarero Espinosa et al. 2013), and that of P-CNCs from tomato plant residue (235–333 °C) (Kassab et al. 2020c), using the same protocol. These results indicate strongly that the thermal behavior of P-CNCs is related to the origin and type of cellulose fibers. Effectively, the higher thermal stability of P-CNCs makes it a potential candidate, as a reinforcement in the development of thermally stable nanocomposite films.

Conclusion

Giant Reed (GR) plant has been valorized for the first time to produce phosphorylated cellulosic materials. Cellulose microfibers (CMFs) were extracted through alkali and bleaching treatments of raw GR, with an average yield and diameter of 37% and 13 μm, respectively. Then, two different phosphorylation processes with and without urea have been performed for the preparation of phosphorylated micro (P-CMFs) and nano (P-CNCs) cellulose. With urea, a higher

surface charge content (CC) was found. The prepared P-CMFs showed a micro-sized shape with an average diameter of 15 μm and a CC of 3133 mmol kg^{-1}. While the extracted P-CNCs exhibited a needle-like shape with an important aspect ratio of (L/D) = 33 and very low CC of 254 mmol kg^{-1}. FTIR analysis confirmed the total removal of non-cellulosic compounds from the surface of microfibers, as well as their partial oxidation after phosphorylation. The cellulose I crystalline structure has been confirmed for all samples, with a slight decrease in the crystallinity index of P-CMFs (70%) compared to that of CMFs (73%) due to the presence of high CC. P-CNCs showed a similar crystallinity index of 83% to that of microcrystalline cellulose (MCC). The TGA analysis showed high thermal behavior for P-CNCs with early dehydration and high char content for P-CMFs.

From these results, we expect that the use of P-CNCs as reinforcement in nanocomposite development will be very beneficial due to its important aspect ratio, high thermal stability, high crystallinity and the ability of phosphate groups to improve the antibacterial properties. P-CMFs may be useful in developing fire-retardant materials due to its high CC leading to early thermal dehydration with rapid char formation. Regarding the diverse potential use of phosphorylated cellulose, it is motivating to produce micro- and nanocellulose from sustainable and inexpensive source as GR plant with the aim of valorizing unexploited Moroccan natural resources.

References

Ait Benhamou A, Boussetta A, Nadifiyine M, Moubarik A (2021) Effect of alkali treatment and coupling agent on thermal and mechanical properties of Opuntia Ficus-Indica cladodes fibers reinforced HDPE composites. Polym Bull. https://doi.org/10.1007/s00289-021-03619-8

Aoki D, Nishio Y (2010) Phosphorylated cellulose propionate derivatives as thermoplastic flame resistant/retardant materials: influence of regioselective phosphorylation on

their thermal degradation behaviour. Cellulose 17:963–976. https://doi.org/10.1007/s10570-010-9440-8

Athukoralalage SS, Balu R, Dutta NK, Choudhury NR (2019) 3D bioprinted nanocellulose-based hydrogels for tissue engineering applications: a brief review. Polymers (Basel) 11:1–13. https://doi.org/10.3390/polym11050898

Baek J, Wahid-pedro F, Kim K et al (2018) Phosphorylated-CNC/modified-chitosan nanocomplexes for the stabilization of pickering emulsions. Carbohydr Polym 206:520–527. https://doi.org/10.1016/j.carbpol.2018.11.006

Bahloul A, Kassab Z, Bouchti M, El et al (2020) Micro- and nano-structures of cellulose from eggplant plant (*Solanum melongena* L.) agricultural residue. Carbohydr Polym 253:117311. https://doi.org/10.1016/j.carbpol.2020.117311

Barana D, Salanti A, Orlandi M et al (2016) Biorefinery process for the simultaneous recovery of lignin, hemicelluloses, cellulose nanocrystals and silica from rice husk and Arundo donax. Ind Crop Prod 86:31–39. https://doi.org/10.1016/j.indcrop.2016.03.029

Beroual M, Boumaza L, Mehelli O et al (2021) Physicochemical properties and thermal stability of microcrystalline cellulose isolated from esparto grass using different delignification approaches. J Polym Environ 29:130–142. https://doi.org/10.1007/s10924-020-01858-w

Bessa W, Tarchoun AF, Trache D, Derradji M (2021) Preparation of amino-functionalized microcrystalline cellulose from Arundo donax L. and its effect on the curing behavior of bisphenol Abased benzoxazine. Thermochim Acta. https://doi.org/10.1016/j.tca.2021.178882

Boussetta A, Ait Benhamou A, Barba FJ et al (2021) Experimental and theoretical investigations of lignin-urea-formaldehyde wood adhesive: Density functional theory analysis. Int J Adhes Adhes 104:102737. https://doi.org/10.1016/j.ijadhadh.2020.102737

Camarero Espinosa S, Kuhnt T, Foster EJ, Weder C (2013) Isolation of thermally stable cellulose nanocrystals by phosphoric acid hydrolysis. Biomacromolecules 14:1223–1230. https://doi.org/10.1021/bm400219u

Cheng M, Qin Z, Hu J et al (2020) Facile and rapid one-step extraction of carboxylated cellulose nanocrystals by H2SO4/HNO3 mixed acid hydrolysis. Carbohydr Polym 231:115701. https://doi.org/10.1016/j.carbpol.2019.115701

Cudjoe E, Hunsen M, Xue Z et al (2017) Miscanthus giganteus: a commercially viable sustainable source of cellulose nanocrystals. Carbohydr Polym 155:230–241. https://doi.org/10.1016/j.carbpol.2016.08.049

Dos Santos ZM, Caroni ALPF, Pereira MR et al (2009) Determination of deacetylation degree of chitosan: a comparison between conductometric titration and CHN elemental analysis. Carbohydr Res 344:2591–2595. https://doi.org/10.1016/j.carres.2009.08.030

Dufresne A (2019) Nanocellulose processing properties and potential applications. Curr For Rep 5:76–89. https://doi.org/10.1007/s40725-019-00088-1

Fernando AL, Barbosa B, Costa J, Papazoglou EG (2016) Giant reed (*Arundo donax* L.): a multipurpose crop bridging phytoremediation with sustainable bioeconomy. In: Bioremediation and bioeconomy. Elsevier, pp 77–95

Fiore V, Scalici T, Valenza A (2014) Characterization of a new natural fiber from *Arundo donax* L. as potential reinforcement of polymer composites. Carbohydr Polym 106:77–83. https://doi.org/10.1016/j.carbpol.2014.02.016

Fiss BG, Hatherly L, Stein RS, Fris T (2019) Mechanochemical phosphorylation of polymers and synthesis of flame-retardant cellulose nanocrystals. ACS Sustain Chem Eng 7:7951–7959. https://doi.org/10.1021/acssuschemeng.9b00764

Flauzino Neto WP, Silvério HA, Dantas NO, Pasquini D (2013) Extraction and characterization of cellulose nanocrystals from agro-industrial residue-Soy hulls. Ind Crops Prod 42:480–488. https://doi.org/10.1016/j.indcrop.2012.06.041

Fortunati E, Puglia D, Monti M et al (2013) Extraction of cellulose nanocrystals from *Phormium tenax* fibres. J Polym Environ. https://doi.org/10.1007/s10924-012-0543-1

Fujisawa S, Zhang J, Saito T et al (2014) Cellulose nanofibrils as templates for the design of poly(L-lactide)-nucleating surfaces. Polymer. https://doi.org/10.1016/j.polymer.2014.04.019

Ghanadpour M, Carosio F, Larsson PT, Wågberg L (2015) Phosphorylated cellulose nanofibrils: a renewable nano-material for the preparation of intrinsically flame-retardant materials. Biomacromolecules 16:3399–3410. https://doi.org/10.1021/acs.biomac.5b01117

Giudicianni P, Cardone G, Sorrentino G, Ragucci R (2014) Hemicellulose, cellulose and lignin interactions on *Arundo donax* steam assisted pyrolysis. J Anal Appl Pyrol 110:138–146. https://doi.org/10.1016/j.jaap.2014.08.014

Gong J, Li J, Xu J (2017) Cellulose sources with various polymorphs. RSC Adv 7:33486–33493. https://doi.org/10.1039/C7RA06222B

Granja P, Pouységu L, Pétraud M et al (2001) Cellulose phosphates as biomaterials. I. Synthesis and characterization of highly phosphorylated cellulose gels. J Appl Polym Sci. https://doi.org/10.1002/app.2193

Illy N, Fache M, Ménard R et al (2015) Phosphorylation of bio-based compounds: state of the art. Polym Chem 6:6257–6291. https://doi.org/10.1039/C5PY00812C

Isik M, Sardon H, Mecerreyes D (2014) Ionic liquids and cellulose: dissolution, chemical modification and preparation of new cellulosic materials. Mol Sci 15:11922–11940. https://doi.org/10.3390/ijms150711922

Jiao Y, Wan C, Qiang T, Li J (2016) Synthesis of superhydrophobic ultralight aerogels from nanofibrillated cellulose isolated from natural reed for high-performance adsorbents. Appl Phys A 122:686. https://doi.org/10.1007/s00339-016-0194-5

Kadimi A, Benhamou K, Habibi Y et al (2016) Nanocellulose alignment and electrical properties improvement. In: Multifunctional polymeric nanocomposites based on cellulosic reinforcements. Elsevier, pp 343–376

Kassab Z, Aziz F, Hannache H et al (2019a) Improved mechanical properties of k-carrageenan-based nanocomposite films reinforced with cellulose nanocrystals. Int J Biol Macromol 123:1248–1256. https://doi.org/10.1016/j.ijbiomac.2018.12.030

Kassab Z, Ben youcef H, Hannache H, El Achaby M (2019b) Isolation of cellulose nanocrystals from various lignocellulosic materials: physico-chemical characterization and

application in polymer composites development. Mater Today Proc 13:964–973. https://doi.org/10.1016/j.matpr.2019.04.061

Kassab Z, Boujemaoui A, Ben Youcef H et al (2019c) Production of cellulose nanofibrils from alfa fibers and its nanoreinforcement potential in polymer nanocomposites. Cellulose 26:9567–9581. https://doi.org/10.1007/s10570-019-02767-5

Kassab Z, Abdellaoui Y, Salim MH et al (2020a) Micro- and nano-celluloses derived from hemp stalks and their effect as polymer reinforcing materials. Carbohydr Polym 245:116506. https://doi.org/10.1016/j.carbpol.2020.116506

Kassab Z, Abdellaoui Y, Salim MH, Achaby M (2020b) Cellulosic materials from pea (*Pisum sativum*) and broad beans (*Vicia faba*) pods agro-industrial residues. Mater Lett 280:128539. https://doi.org/10.1016/j.matlet.2020.128539

Kassab Z, Kassem I, Hannache H et al (2020c) Tomato plant residue as new renewable source for cellulose production: extraction of cellulose nanocrystals with different surface functionalities. Cellulose 27:4287–4303. https://doi.org/10.1007/s10570-020-03097-7

Kawaguchi S, Yekta A, Winnik M (1995) Surface characterization and dissociation properties of carboxylic acid core–shell latex particle by potentiometric and conductometric titration. J Colloid Interface Sci 167:362–369

Kokol V, Bozic M, Vogrincic R, Mathew AP (2015) Characterisation and properties of homo- and heterogenously phosphorylated nanocellulose. Carbohydr Polym 125:301–313. https://doi.org/10.1016/j.carbpol.2015.02.056

Lavoine N, Desloges I, Dufresne A, Bras J (2012) Microfibrillated cellulose: its barrier properties and applications in cellulosic materials: a review. Carbohydr Polym 90:735–764. https://doi.org/10.1016/j.carbpol.2012.05.026

Lehtonen J, Hassinen J, Kumar AA et al (2020) Phosphorylated cellulose nanofibers exhibit exceptional capacity for uranium capture. Cellulose 27:10719–10732. https://doi.org/10.1007/s10570-020-02971-8

Lewandowski I, Scurlock JMO, Lindvall E, Christou M (2003) The development and current status of perennial rhizomatous grasses as energy crops in the US and Europe. Biomass Bioeng 25:335–361. https://doi.org/10.1016/S0961-9534(03)00030-8

Liao JJ, Abd Latif NH, Trache D et al (2019) Current advancement on the isolation, characterization and application of lignin. Int J Biol Macromol 162:985–1024. https://doi.org/10.1016/j.matdes.2019.108334

Liu P, Borrell PF, Božič M et al (2015) Nanocelluloses and their phosphorylated derivatives for selective adsorption of Ag^+, Cu^{2+} and Fe^{3+} from industrial effluents. J Hazard Mater 294:177–185. https://doi.org/10.1016/j.jhazmat.2015.04.001

Mahmud MM, Perveen A, Jahan RA et al (2019) Preparation of different polymorphs of cellulose from different acid hydrolysis medium. Int J Biol Macromol 130:969–976. https://doi.org/10.1016/j.ijbiomac.2019.03.027

Noguchi Y, Homma I, Matsubara Y (2017) Complete nanofibrillation of cellulose prepared by phosphorylation. Cellulose 24:1295–1305. https://doi.org/10.1007/s10570-017-1191-3

Reid D, Laurence W, Mazzeno J (1949) Preparation and properties of cellulose phosphates. Ind Eng Chem 41:2828–2831

Rol F, Belgacem N, Meyer V et al (2019) Production of fire-retardant phosphorylated cellulose fibrils by twin-screw extrusion with low energy consumption. Cellulose 26:5635–5651. https://doi.org/10.1007/s10570-019-02447-4

Rol F, Sillard C, Bardet M et al (2020) Cellulose phosphorylation comparison and analysis of phosphorate position on cellulose fibers. Carbohydr Polym 229:115294. https://doi.org/10.1016/j.carbpol.2019.115294

Segal L, Creely L, Martin AE, Conrad M (1958) Empirical method for estimating the degree of crystallinity of native cellulose using the X-ray diffractometer. Text Res J 29:786–794. https://doi.org/10.1177/004051755902901003

Silva CFLe, Schirmer MA, Maeda RN et al (2014) Potential of giant reed (*Arundo donax* L.) for second generation ethanol production. Electron J Biotechnol 18:1–6. https://doi.org/10.1016/j.ejbt.2014.11.002

Siqueira G, Kokkinis D, Libanori R et al (2017) Cellulose nanocrystal inks for 3D printing of textured cellular architectures. Adv Funct Mater 27:1604619. https://doi.org/10.1002/adfm.201604619

Suflet DM, Chitanu GC, Popa VI (2006) Phosphorylation of polysaccharides: new results on synthesis and characterisation of phosphorylated cellulose. React Funct Polym 66:1240–1249. https://doi.org/10.1016/j.reactfunctpolym.2006.03.006

Tang Y, Shen X, Zhang J et al (2015) Extraction of cellulose nano-crystals from old corrugated container fiber using phosphoric acid and enzymatic hydrolysis followed by sonication. Carbohydr Polym 125:360–366. https://doi.org/10.1016/j.carbpol.2015.02.063

Tarchoun AF, Trache D, Klapotke TM et al (2019a) Ecofriendly isolation and characterization of microcrystalline cellulose from giant reed using various acidic media. Cellulose 26:7635–7651. https://doi.org/10.1007/s10570-019-02672-x

Tarchoun AF, Trache D, Klapötke TM (2019) Microcrystalline cellulose from *Posidonia oceanica* brown algae: extraction and characterization. Int J Biol Macromol 138:837–845. https://doi.org/10.1016/j.ijbiomac.2019.07.176

Tian H, He J (2016) Cellulose as a scaffold for self-assembly: from basic research to real applications. Langmuir 32:12269–12282. https://doi.org/10.1021/acs.langmuir.6b02033

Trache D, Hussin MH, Haafiz M, Thakur VK (2017) Recent progress in cellulose nanocrystals: sources and production. Nanoscale 9:1763–1786. https://doi.org/10.1039/c6nr09494e

Trache D (2018) Nanocellulose as a promising sustainable material for biomedical applications. AIMS Mater Sci 5(2):201–205. https://doi.org/10.3934/matersci.2018.2.201

Trache D, Tarchoun AF, Derradji M, Hamidon TS (2020a) Nanocellulose: from fundamentals to advanced

applications. Front Chem 8:392. https://doi.org/10.3389/fchem.2020.00392

Trache D, Thakur VK, Boukherroub R (2020b) Cellulose nanocrystals/graphene hybrids: a promising new class of materials for advanced applications. Nanomaterials 10:1523. https://doi.org/10.3390/nano10081523

Zhang PP, Tong DS, Lin CX et al (2014) Effects of acid treatments on bamboo cellulose nanocrystals. Asia Pac J Chem Eng 9:686–695. https://doi.org/10.1002/apj